Composites Science and Technology 198 (2020) 108283

Contents lists available at ScienceDirect

Composites Science and Technology

journal homepage: http://www.elsevier.com/locate/compscitech

Ultra-thin and ultra-strong organic interphase in nanocomposites with supercrystalline particle arrangement: Mechanical behavior identification via multiscale numerical modeling

Mingjing Li [a,*], Ingo Scheider [a], Büsra Bor [b], Berta Domènech [b], Gerold A. Schneider [b], Diletta Giuntini [b,**]

[a] Institute of Materials Research, Materials Mechanics, Helmholtz-Zentrum Geesthacht, Germany
[b] Hamburg University of Technology, Institute of Advanced Ceramics, Hamburg, Germany

ARTICLE INFO

Keywords:
Nano composites
Interphase
Mechanical properties
Multiscale modeling
Sensitivity study

ABSTRACT

A key challenge in the development of inorganic-organic nanocomposites is the mechanical behavior identification of the organic phase. For supercrystalline materials, in which the organic phase ranges down to sub-nm areas, the identification of the organic materials' mechanical properties is however experimentally inaccessible. The supercrystalline nanocomposites investigated here are 3D superlattices of self-assembled iron oxide nanoparticles, surface-functionalized with crosslinked oleic acid ligands. They exhibit the highest reported values of Young's modulus, nanohardness and strength for inorganic-organic nanocomposites. A multiscale numerical modeling approach is developed to identify these properties using supercrystalline representative volume elements, in which the nanoparticles are arranged in a face-centered cubic superlattice and the organic phase is modeled as a thin layer interfacing each particle. A Drucker-Prager-type elastoplastic constitutive law with perfectly plastic yielding is identified as being able to describe the supercrystals' response in nanoindentation accurately. As the nanoparticles behave in a purely elastic manner with very high stiffness, the underlying constitutive law of the organic phase is also identified to be Drucker-Prager-type elastoplastic, with a Young's modulus of 13 GPa and a uniaxial tensile yield stress of 900 MPa, remarkably high values for an organic material, and matching well with experimental and DFT-based estimations. Furthermore, a sensitivity study indicates that small configurational changes within the supercrystalline lattice do not significantly alter the overall stiffness behavior. Multiscale numerical modeling is thus proven to be able to identify the nanomechanical properties of supercrystals, and can ultimately be used to tailor these materials' mechanical behavior starting from superlattice considerations.

1. Introduction

Structurally-ordered nanocomposites are emerging as key building blocks for the multiscale assembly of hierarchical materials systems with encoded functionality, amplified by new couplings between electrical, optical, transport, and mechanical properties [1]. In such a rising field of materials engineering, the processing and assembly of mechanically robust supercrystalline ceramic-organic nanocomposites become decisive. Several approaches have been optimized for the development of self-assembled nanocomposites, leading to a wide spectrum of available techniques and potential applications [2–6]. The mechanical properties of the resulting materials typically reach the values characteristic of hard polymers, and there is general agreement on the important role played by the supercrystallinity in enhancing the nanocomposites' strength, hardness and stiffness [7–10].

More recently, it has been shown that these kinds of supercrystalline nanocomposites are capable of reaching an impressive combination of mechanical properties, with hardness up to 5 GPa, Young's modulus up to 70 GPa, and compressive strength above 1 GPa [11,12]. In such nanocomposites, the organic ligands are anchored to the ceramic nanoparticles, which are self-assembled in an FCC (face-centered cubic) superlattice. The crosslinking of the organic ligands is identified as

* Corresponding author.
** Corresponding author.
E-mail addresses: mingjing.li@hzg.de (M. Li), diletta.giuntini@tuhh.de (D. Giuntini).

https://doi.org/10.1016/j.compscitech.2020.108283
Received 11 March 2020; Received in revised form 29 April 2020; Accepted 4 June 2020
Available online 10 June 2020
0266-3538/© 2020 The Authors. Published by Elsevier Ltd. This is an open access article under the CC BY license (http://creativecommons.org/licenses/by/4.0/).

responsible for such an enhancement of the nanocomposites' mechanical behavior. Crosslinking is induced by a heat treatment at temperatures in the 250 − 350°C range and leads to the formation of covalent bonds among interdigitated organic ligands. The organic phase achieves therefore a unique configuration, being highly confined into a sub-nm layer interfacing the ceramic nanoparticles, anchored to the latter and crosslinked through the various chains. This implies a very high stiffness for a material (oleic acid) that would otherwise be a liquid at room temperature. While the physical properties of the free oleic acid are known, the ones of the corresponding coordinated and confined oleate are not. The assessment of the details of this ligand's mechanical properties is extremely cumbersome – if not impossible – to achieve experimentally [13–15].

Numerical modeling is the ideal solution to overcome such experimental limitations. To access information on the role of the confined organic ligands towards the overall mechanical response of the supercrystalline nanocomposites, an efficient approach is found in continuum micromechanical modeling. Even though the organic phase (often named interphase in the literature [16,17]) exhibits a discrete molecular structure on the nanometer scale [18], continuum micromechanical modeling can provide robust predictions of the effective behavior of the nanocomposites, if a reliable multiscale modeling strategy is used to account for the intrinsically hierarchical material morphology [19–23]. In the recent years, indeed, continuum-based multiscale modeling approaches have been applied intensively, in combination with FEM (finite-element method), to explore the stiffness behavior [24–28] and failure mechanisms [29–31] of nanocomposites, with particular interest for the role played by their nanostructures, *i.e.* size and spatial distribution of inclusions, as well as interphase thickness.

For the supercrystalline nanocomposites of interest in this work, a nonlocal damage model based on a micropolar continuum theory has been proposed in a previous work [32]. This approach focused on the inelastic and damage behavior of the crosslinked organic interphase, and was validated through experimental results from bending tests of microbeams [11]. However, for such a sophisticated material model, a very large number of material parameters is required, which cannot be uniquely identified via numerical methods from the limited set of the experimental data that is currently attainable. A simpler modeling approach has thus been implemented here, capable on the one hand to unequivocally determine all the needed input material parameters from experimental results, and, on the other hand, to reliably derive both stiffness and strength of the confined and crosslinked organic interphase in supercrystalline nanocomposites. It turns out that the overall (macroscopically homogenized) mechanical behavior is accurately described by a linear elastic-perfectly plastic material model.

This model is capable to predict the experimentally measured nanoindentation hardness, load-displacement curves, and the associated material deformations [12]. By means of properly-defined supercrystalline RVEs (representative volume elements), a multiscale FE (finite-element) modeling approach is developed to derive the mechanical properties of the organic interphase. Since the organic ligands present in the system are short aliphatic chains (oleic acid, $C_{18}H_{34}O_2$), the ceramic nanoparticles in the supercrystalline RVEs are not considered as embedded in an organic matrix, but rather interfaced by the thin confined interphase and with hollow superlattice interstitial sites. An elastoplastic material behavior of the homogenized (continuum) supercrystalline nanocomposites translates into an analogous mechanical response at the local interphase level, while the stronger inorganic (iron oxide) phase behaves in a purely linear elastic fashion. Together with these insights on the behavior of the supercrystalline nanocomposites' phases, remarkable outcomes also emerge on the stiffness and strength that the confined and crosslinked organic interphase can reach. This multiscale modeling approach is finally used to address another issue that typically affects supercrystalline materials, namely the very wide data scatter characteristic of micromechanical testing outcomes [8,11,12]. Such large scatter has been attributed to several causes, among which the presence of supercrystalline defects and the size distribution of the constituent nanoparticles are numerically addressed in this work.

2. Method: multiscale numerical modeling

2.1. RVE of the supercrystalline nanostructure

The material of interest in this work is a bulk supercrystalline nanocomposite with iron oxide nanoparticles (magnetite, Fe_3O_4), surface-functionalized with oleic acid, as constituent building blocks. The iron oxide nanoparticles are self-assembled in the FCC superlattice and the oleic acid molecules are crosslinked, leading to a significant enhancement of the nanocomposite's mechanical properties. Details on material's nanostructure and processing routine are given in SI 1. The nanostructure is here described via an RVE (representative volume element), a geometrical reconstruction of the organically-functionalized ceramic nanoparticles' arrangement within the superlattice.

A transmission electron microscopy (TEM) image of the superlattice is shown in Fig. 1, where the supercrystalline nanostructure and the interphase's presence can be observed. The micrograph was taken along the (112) projection axis of the nanocomposite's FCC superlattice, and {111} planes can be identified running diagonally through the image. Based on the supercrystalline nanostructure, the RVE is defined, as shown in Fig. 1, by three parameters: nearest neighbor distance $NND = 18.4$ nm, minimum inter-particle distance $ID = 0.6$ nm, and interphase thickness $IT = 1.1$ nm, as detailed in SI 2.

Note that, although bulk oleic acid is liquid at room temperature, its behavior is here significantly altered, due to the anchoring on the iron oxide surfaces, the sub-nm confinement and the crosslinking process triggered by the heat treatment. The oleic acid interphase is therefore considered as a solid phase with uniform thickness in the RVE filling the gap between nanoparticles. Additionally, crosslinked oleic acid molecules are directly anchored to the iron oxide nanoparticles and no solvent is left in the nanocomposites after the heat treatment [11], and thus, as verified in SI 3, the interstitial sites in the RVE are considered to be hollow.

After synthesis, the nanoparticles are quasi-spherical [11], thus, for the RVE, a reasonable option is modeling them as spheres (SPHER RVE, Fig. 2(a)). Note that symmetry conditions allow considering only 1/8 of each RVE when loading is applied parallel to the cube axes. A potential alternative is a cuboctahedral shape, based on nanoparticle synthesis considerations, and on DFT (density functional theory) studies [33]. RVEs with cuboctahedral nanoparticles (CUBO RVEs, Fig. 2(b)), are thus also considered, to evaluate which nanoparticle morphology leads to a better match with experimental data, and thus can be considered most representative of heat-treated supercrystals.

In the supercrystalline nanocomposites, the iron oxide (indexed IO) phase is the strong inorganic phase, and it is therefore modeled as linear elastic with parameters extracted from the literature: Young's modulus $E_{IO} = 163$ GPa and Poisson's ratio $\nu_{IO} = 0.3$ [34]. The oleic acid phase is the nanocomposites' soft phase, and it is assumed to undergo significant permanent deformations upon mechanical loading. An elastoplastic behavior is thus selected for the organic interphase. Note that the combination of a purely elastic and an elastoplastic phase in the supercrystalline nanocomposites implies that the overall homogenized composite is also behaving in an elastoplastic manner. In this work, the Drucker-Prager yield function is selected, since it is able to capture experimentally-detected aspects of the nanocomposites' mechanical behavior. These are presence of inelastic deformations (leading to overall nonlinear behavior in the nanocomposites), different values of tensile and compressive strengths [11], and the pressure-sensitivity typical of organic matrices in composites [35–37]. Both interphase (oleic acid, indexed OA) and nanocomposites (supercrystalline, indexed SC) are thus described via four parameters each: Young's modulus (E), Poisson's ratio (ν), and two plastic parameters for the Drucker-Prager

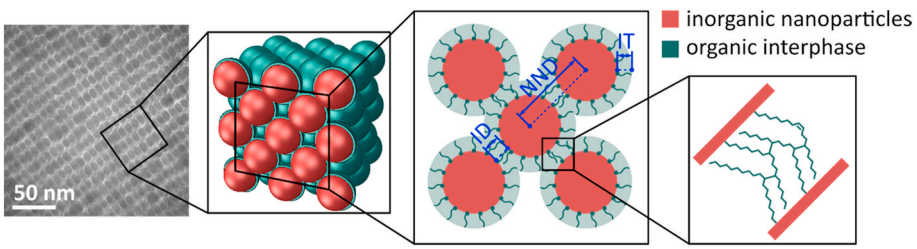

Fig. 1. From left to right: TEM micrograph of the nanocomposite's superlattice taken along the (112) direction; model of supercrystalline nanostructure and 2D view with the definition of geometric parameters - *NND* (nearest neighbor distance), *ID* (minimum inter-particle distance), and *IT* (interphase thickness); close-up representation of the nanoparticle's surface with crosslinked ligands.

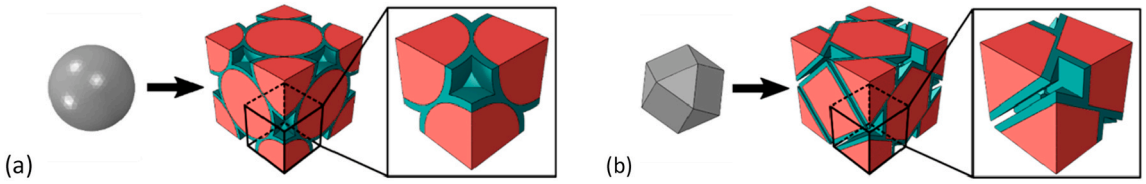

Fig. 2. (a) SPHER and (b) CUBO RVEs of the supercrystalline nanocomposites, and the corresponding simplified RVE defined according to symmetric conditions.

yield function (cohesion c and friction angle φ). Details on the models are given in SI 4.

2.2. Multiscale strategy

The supercrystalline nanocomposites' mechanical properties can be probed experimentally starting from the microscale upwards, while experimental methods for characterizing the mechanical properties of the constituent phases on the sub-nm or nm scale are not available [13]. Therefore, a multiscale FE modeling approach is implemented, to bridge the nanoscopic superlattice with the overall macroscopic nanocomposite response, and subsequently access the information that is experimentally unattainable. The multiscale modeling strategy is schematically illustrated in Fig. 3. The material parameters are iteratively identified at these various scales. The supercrystalline RVE defined in the previous section constitutes the basic unit cell of a homogenized material element, which is in turn a representative of the overall continuum behavior of the macroscopic material. The test of choice for experimental validation is nanoindentation, due to the availability of a broad and detailed set of data [12].

The starting point for the multiscale strategy is the homogenized material element capturing the effective nanocomposite behavior on the micrometer scale. Nanoindentation is numerically simulated on this homogeneous continuum, after having selected the most suitable constitutive description of the material. Details on the nanoindentation model are given in SI 5. The material parameters are then identified based on the comparison between experimental and numerical results.

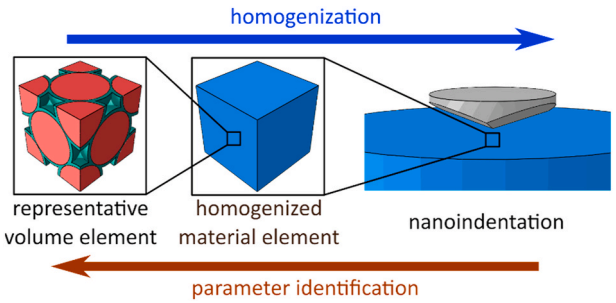

Fig. 3. Multiscale strategy to identify interphase properties in RVEs of the superlattice and the homogenized properties of the supercrystalline nanocomposite, using experimental results from nanoindentation tests as reference.

Once the homogenized properties of the specimen are derived and validated, the parameter identification step allows zooming back into the supercrystalline lattice, down to the RVE on the nanometer scale, where the material parameters related to the crosslinked and confined organic ligands can be identified.

3. Results and discussion

3.1. Homogenized nanocomposite behavior: nanoindentation modeling

A previous experimental nanoindentation campaign was used as reference to validate the proposed numerical approach and to extract additional information on the mechanical behavior of the homogenized supercrystalline nanocomposites [12]. In the experimental study, a Berkovich indenting tip has been used to investigate stiffness and hardness of the nanocomposites, and this test is here reproduced via FE simulations (see SI 5). The material parameters of the homogenized supercrystalline nanocomposites (SC) are identified as follows.

The uniaxial compressive strength $\sigma_{SC,c} = 1.161$ GPa, determined from microcompression tests, is employed as a known parameter. The Poisson's ratio of the nanocomposite is assumed to be $\nu_{SC} = 0.3$ since it cannot be determined unequivocally from nanoindentation tests. The impact of the organic material's behavior on the homogenized Poisson's ratio will be discussed later. Thus, the homogenized material parameters to be identified from the nanoindentation modeling are the Young's modulus E_{SC} and the uniaxial tensile strength $\sigma_{SC,t}$. As a first step, the nanocomposite's Young's modulus is determined based on the unloading slope at maximum force of the nanoindentation force-displacement curves. By fitting the slope of the numerical curve to the averaged slope of experimental curves (see Fig. 4), a value of $E_{SC} = 50$ GPa is found. As a second step, the uniaxial tensile strength, $\sigma_{SC,t} = 850$ MPa, is determined when the maximum indentation force obtained numerically matches its averaged experimental value. With this, the parameters for the Drucker-Prager yield function are then derived as friction angle $\varphi_{SC} = 25^\circ$ and cohesion $c_{SC} = 981$ MPa. By using the identified parameters, excellent agreement is found with experiments, in terms of the nanoindentation force-displacement curves (see Fig. 4) and hardness, which reads $H_{SC} = 4.78$ GPa from numerical modeling and $\widehat{H}_{SC} = 4.72$ GPa from experimental tests. One can therefore conclude that the material parameters are properly identified. Note that the numerically identified Young's modulus $E_{SC} = 50$ GPa is different from the experimental value $\widehat{E}_{SC} = 64.1$ GPa [12]. The reason of this mismatch is

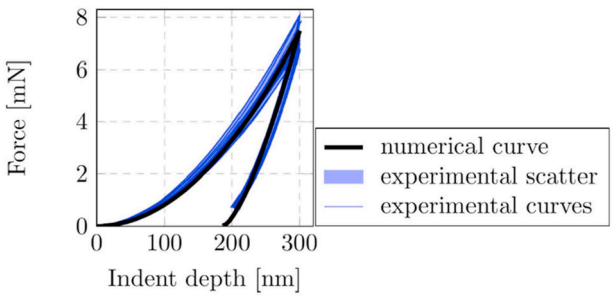

Fig. 4. Comparison of numerical and experimental nanoindentation force-displacement curves.

discussed in terms of the nanoindentation model's details in SI 5.

3.2. Ultra-thin organic interphase behavior: RVE-based modeling

The homogenized material behavior described above is used to identify the interphase properties of the geometrically-confined and crosslinked oleic acid phase, using supercrystalline RVEs. Details about FE implementations of RVE-based modeling are given in SI 2. The interphase Young's modulus E_{OA} and Poisson's ratio ν_{OA} are the first to be identified. The optimal interphase Young's modulus E_{OA} is found by imposing that the RVE's effective Young's modulus E_{RVE} equals the value of the homogenized nanocomposite, $E_{SC} = 50$ GPa. Fig. 5(a) shows the correlation among E_{RVE} and E_{OA} for SPHER and CUBO RVEs. Note that the SPHER RVE is isotropic, while the CUBO RVE has transversely isotropic behavior (with Z as out-of-plane direction and X–Y plane as plane of isotropy). Since neither the interphase's nor the nanocomposite's Poisson's ratio is known, the other parameter taken into consideration is the interphase Poisson's ratio, by considering $\nu_{OA}^{C} = 0.3$ and $\nu_{OA}^{I} = 0.495$ (compressible and quasi-incompressible case).

All of these possible RVE configurational combinations are presented in Fig. 5(a). Note that a broad range of potential values of interphase Young's modulus is plotted, to show its relation to the effective ones of the nanocomposite. However, based on previous studies [11,38], the most suitable interval for E_{OA} is $10 - 15$ GPa. This is a rather high value for an organic material, but considering its short chains' high confinement in a sub-nm space, the rigid anchoring to the iron oxide surfaces and the covalent crosslinking, such a range is plausible. By intersecting the nanocomposite's Young's modulus (50 GPa) with the curves relative to E_{OA} and considering this range, two options are found: $E_{OA}^{I,\,CUBO} = 14.5$ GPa and $E_{OA}^{I,\,SPHER} = 13$ GPa (both with quasi-incompressible interphase), as marked by black dots in Fig. 5(a). Because of the absence, or very minor incidence, of nanoparticle faceting for samples heat-treated at 325°C [39], the SPHER RVE is selected. Note that, in a previous work conducted with heat treatment at 350°C [11], faceting was instead observed via high-resolution TEM (HRTEM), and a CUBO RVE should thus be considered for this kind of material. Faceting, in turn, would likely lead to interlocking effects, contributing to the further material strengthening when higher heat treatment temperatures are applied [40].

Modeling the geometrically confined oleic acid interphase as incompressible, however, does not imply incompressibility of the nanocomposites, since the interstitial sites of the FCC lattice are considered as hollow. Experimental data has indeed suggested room for compressibility during indentation of supercrystalline nanocomposites [12]. To better visualize this effect, the impact of the interphase Young's modulus (E_{OA}) and Poisson's ratio (ν_{OA}) on the effective RVE's Poisson's ratio (ν_{RVE}) is shown in Fig. 5(b). It emerges that the interphase Young's modulus E_{OA} plays a minor role. For the selected configuration – spherical nanoparticles with incompressible interphase, $\nu_{RVE} = 0.34$ is found. Note that the transversely isotropic behavior of the CUBO model leads to a relatively wide range of ν_{RVE} values, but this property spread fades when the average among in-plane and out-of-plane values is taken (dashed curves). These CUBO RVE outcomes suggest however that if the supercrystals' constituent nanoparticles do feature faceting, the numerically-obtained in-plane and out-of-plane behaviors can be considered as the extreme cases, resulting in lower and upper boundaries of the nanocomposites' real behavior.

Now that the interphase elastic parameters have been obtained - $E_{OA} = 13$ GPa and $\nu_{OA} = 0.495$ - the plasticity parameters can be identified. Based on the multiscale modeling strategy (see Fig. 3), this step is performed by assimilating the effective stress-strain curves from the homogenized material element (HOMO) with the RVEs (RVE), as shown in Fig. 6. These outcomes are relative to the selected SPHER-I model (spherical nanoparticles and incompressible interphase). Compressive and tensile behaviors are both considered, as experimental work on micropillar tests (pure compression) and micro-bending (combined compression and tension) shows an asymmetry in the supercrystalline nanocomposites' response when subjected to these two loading conditions [11].

Fig. 6(a) shows the stress-strain curves, under both uniaxial tension and compression conditions, of the homogenized material element and of the supercrystalline RVE. A good agreement is found, allowing to move forward to the derivation of the RVE components' parameters, namely the Drucker-Prager parameters for the oleic acid. These are identified as $c_{OA} = 932$ MPa and $\varphi_{OA} = 6°$, and the corresponding uniaxial tensile and compressive yield stresses become $\sigma_{OA,t} = 900$ MPa and $\sigma_{OA,c} = 965$ MPa. The higher compressive strength with respect to the tensile one is also observed experimentally [11]. The stress-strain curves for the oleic acid interphase (OA) are plotted in Fig. 6(b).

Note that the values for the Young's modulus and the strength of the oleic acid are exceptionally high for an organic material, but still

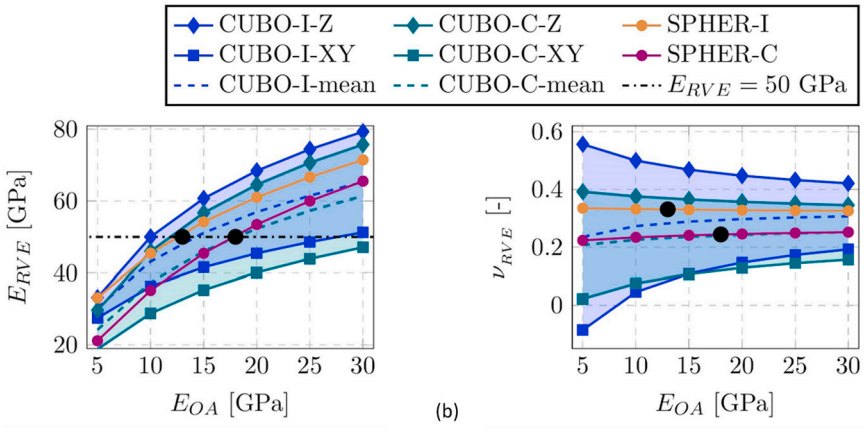

Fig. 5. Dependence of (a) effective Young's modulus E_{RVE} and (b) effective Poisson's ratio ν_{RVE} of supercrystalline RVEs with respect to Young's modulus E_{OA} and Poisson's ratio ν_{OA} of the interphase, for both the SPHER and CUBO RVEs. Both compressible ($\nu_{OA}^{C} = 0.3$) and quasi-incompressible ($\nu_{OA}^{I} = 0.495$) interphase behaviors are studied, here denoted as C and I, respectively. For the CUBO RVE, XY and Z refer to the in-plane and out-of-plane Young's modulus, and their mean value is plotted with dashed curves.

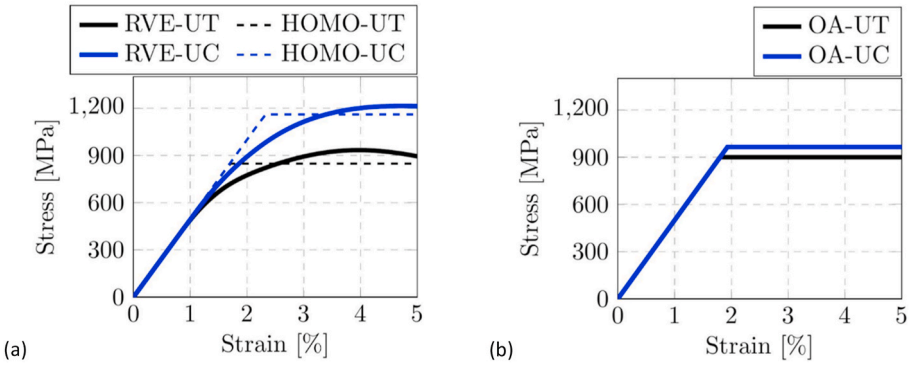

Fig. 6. Numerically obtained stress-strain curves for (a) the homogenized material element (HOMO) and the SPHER RVE (RVE), and (b) the corresponding interphase behavior (OA), under uniaxial tensile (UT) and compressive (UC) loading conditions.

expected from an analysis of experimental micromechanical data and DFT calculations [11,41], especially for such small stress-transferring areas through the interphase (see SI 6). Such high mechanical properties values can be further validated via a simple model based on molecular considerations. The strength σ_{OA} of the crosslinked oleic acid is related to the breaking force F_{OA} of one oleic acid molecule via the area crosslink density ρ_{cl}, as $\sigma_{OA} = F_{OA}\,\rho_{cl}$, with $F_{OA} \cong 2$ nN [11]. Therefore, with a realistic crosslink density of $\rho_{cl} \cong 0.451$ nm^{-2} [11], a yield stress of 900 MPa is achieved, which is coincident with the numerical outcomes given above. With the same approach, the Young's modulus of the oleic acid can be estimated as $E_{OA} = \rho_{cl}\,\gamma_1$, where $\gamma_1 = 28.7$ nN is the spring constant for alkane molecules with less than 20 carbons (such as oleic acid is) [41]. This results in $E_{OA} \cong 12.9$ GPa, which again fits very well with the Young's modulus derived with our multiscale continuum mechanics-based approach. The Drucker-Prager model is therefore confirmed to provide a very suitable constitutive description for the confined oleic acid. The powerful role of the organic phase's crosslinking, confinement and anchoring to the nanoparticles in altering the material's effective mechanical response is confirmed. It was also verified that the iron oxide nanoparticles undergo negligible plastic deformation, see SI 7.

3.3. Sensitivity to superlattice alterations

Highly-scattered mechanical behavior of supercrystalline nanocomposites has been reported and discussed in a variety of works [8,11,12]. The reason is however still unclear and difficult to experimentally address. A hypothesis is based on the intrinsic imperfections within the supercrystals' FCC arrangement, due to the unavoidable size variations among the nanoparticles [42]. The numerical approach developed here is therefore also employed to assess whether such superlattice irregularities lie behind the results' scattering.

Taking the SPHER-I RVE as reference (see Fig. 7(a)), two different kinds of superlattice imperfections are considered, namely translational shift (see Fig. 7(b)) and size variation (see Fig. 7(c) and (d)) of selected nanoparticles. This study is performed for the elastic part of the material's constitutive behavior, using the interphase elastic parameters derived above ($E_{OA} = 13$ GPa and $\nu_{OA} = 0.495$).

As summarized in Table 1, the effect of variations in the nanoparticles' size has a much stronger effect on the nanocomposite's effective Young's modulus, $13-17\%$, with respect to their positioning within the FCC lattice, around 1%. Details on the analysis of all the three cases are given in SI 8. However, such alternations have opposing sign depending on the size change itself (increase or decrease), and the overall effect of size variations is likely to be self-compensating on the macroscale. These kinds of superlattice alterations are therefore not sufficient to explain the large data scatter that has been experimentally observed, unless varying material batches with different average nanoparticle size are considered, or faceting of the nanoparticles is present (see considerations on CUBO RVEs). Additional work is being conducted in this direction, both experimentally and numerically.

4. Conclusions

A multiscale modeling strategy has been proposed to assess the mechanical behavior of bulk supercrystalline nanocomposites. The simulated material is an iron oxide-oleic acid supercrystalline nanocomposite with crosslinked organic ligands, leading to a remarkable

Table 1
Impact on the effective Young's modulus of the respective configurational changes in the SPHER RVE. Unaltered RVE refers to the perfect supercrystal RVE with monodisperse nanoparticle size. As modified cases, the nanoparticles are either kept monodisperse, but shifted, or kept in their unperturbed positions, but changed in size.

RVE configurations		Young's modulus E	Difference
Unaltered (perfect supercrystal)		49.8 GPa	–
Modified	Shifted particles	49.3 GPa	− 1.0%
	Increasing particle radius (+5%)	58.5 GPa	+ 17.5%
	Decreasing particle radius (−5%)	43.0 GPa	− 13.7%

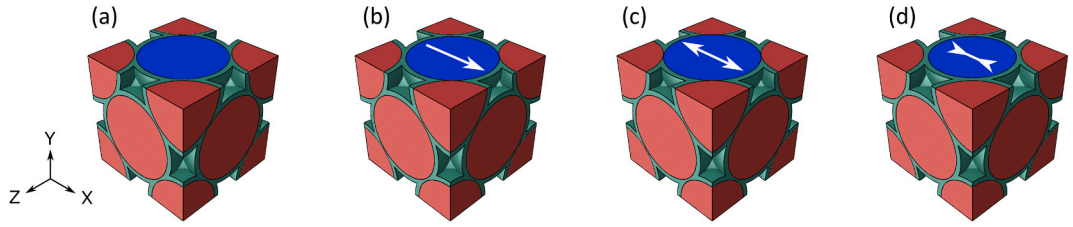

Fig. 7. SPHER RVEs for the following alterations of selected nanoparticles (marked in blue) on the Y- and Y+ surfaces: (a) unaltered; (b) shifting in the X+ direction; (c) increasing the size; (d) decreasing the size. (For interpretation of the references to colour in this figure legend, the reader is referred to the Web version of this article.)

combination of mechanical properties [11,12]. Experimental information on the constitutive behavior of the confined and crosslinked organic phase that interfaces the ceramic nanoparticles, and on the causes underlying the severe data scatter affecting mechanical tests, is, however, still unavailable, and it is here targeted numerically. The implemented numerical approach considers both the face-centered cubic geometry of the supercrystals, with its two material components, and its homogenized macroscopic continuum version. By modeling the ceramic phase as linear elastic and the organic phase as elastoplastic, an excellent agreement between experimental and numerical nanoindentation results is found. The Drucker-Prager yield function, selected to model the plastic response, is able to capture the materials mechanical behavior, while requiring a limited number of input parameters. By matching the macroscopic material properties with the supercrystalline RVE ones, the details of the RVE geometry and organic interphase's properties are extracted. Since the organic interphase is composed by short aliphatic chains, it is modeled as a thin layer interfacing the ceramic nanoparticles in supercrystalline RVEs with hollow interstitial sites. It emerges that the ceramic nanoparticles stay spherical even after the applied heat treatment at 325°C, and that the organic phase is quasi-incompressible, reaching a Young's modulus of 13 GPa and a tensile strength of 900 MPa, thanks to its high confinement, anchoring to the nanoparticles and inter-chains crosslinking. These values show very accurate matching with combined experimental and DFT-based estimations. The nanocomposites' effective Poisson's ratio results to be 0.34, meaning that the empty interstitial sites in the supercrystalline lattice allow moderate compressibility. A parametric sensitivity study was also performed, to check on the effects of varying nanoparticles sizes and positions within the RVE, an issue that always affects supercrystalline materials. The varying nanoparticles positions are shown to play a very minor role, while changing their sizes leads to alterations of the material's effective elastic response in the 13 – 17% range. This last effect is, however, self-compensating, depending on the sign of the nanoparticles' size variations, and is thus not sufficient to justify the wide experimental data scatter. This suggests that larger-scale defects might be playing a role, and numerical and experimental studies are in progress to elucidate this last point.

CRediT authorship contribution statement

Mingjing Li: Conceptualization, Methodology, Software, Validation, Formal analysis, Writing - original draft. **Ingo Scheider:** Conceptualization, Methodology, Writing - review & editing, Supervision, Project administration, Funding acquisition. **Büsra Bor:** Investigation, Writing - review & editing. **Berta Domènech:** Investigation, Writing - review & editing. **Gerold A. Schneider:** Investigation, Writing - review & editing, Project administration, Funding acquisition. **Diletta Giuntini:** Conceptualization, Investigation, Writing - review & editing, Supervision.

Declaration of competing interest

The authors declare that they have no known competing financial interests or personal relationships that could have appeared to influence the work reported in this paper.

Acknowledgements

The authors gratefully acknowledge financial support from the Deutsche Forschungsgemeinschaft (DFG, German Research Foundation) – Projektnummer 192346071 – SFB 986. B.B. gratefully acknowledges the support from the Ministry of National Education of the Republic of Turkey. D.G. gratefully acknowledges the support from the Alexander von Humboldt Foundation. The authors are very thankful to Dr. Malte Blankenburg and Dr. Anton Davydok for their valuable input and cooperation in the SAXS characterization of the materials, and Dr. Tobias Krekeler for his support with transmission electron microscopy, used here as experimental reference.

Appendix A. Supplementary data

Supplementary data to this article can be found online at https://doi.org/10.1016/j.compscitech.2020.108283.

References

[1] M.R. Begley, D.S. Gianola, T.R. Ray, Bridging functional nanocomposites to robust macroscale devices, Science 364 (6447) (2019), eaav4299.
[2] M.A. Boles, M. Engel, D.V. Talapin, Self-assembly of colloidal nanocrystals: from intricate structures to functional materials, Chem. Rev. 116 (18) (2016) 11220–11289.
[3] E.V. Sturm, H. Colfen, Mesocrystals: past, presence, future, Crystals 7 (7) (2017) 207.
[4] M.P. Pileni, Nanocrystal self-assemblies: fabrication and collective properties, J. Phys. Chem. B 105 (17) (2001) 3358–3371.
[5] S.C. Glotzer, M.J. Solomon, Anisotropy of building blocks and their assembly into complex structures, Nat. Mater. 6 (8) (2007) 557–562.
[6] B. Domenech, M. Kampferbeck, E. Larsson, T. Krekeler, B. Bor, D. Giuntini, M. Blankenburg, M. Ritter, M. Muller, T. Vossmeyer, et al., Hierarchical supercrystalline nanocomposites through the self-assembly of organically-modified ceramic nanoparticles, Sci. Rep. 9 (1) (2019) 3435.
[7] E. Tam, P. Podsiadlo, E. Shevchenko, D.F. Ogletree, M.P. Delplancke-Ogletree, P. D. Ashby, Mechanical properties of face-centered cubic supercrystals of nanocrystals, Nano Lett. 10 (7) (2010) 2363–2367.
[8] P. Podsiadlo, G. Krylova, B. Lee, K. Critchley, D.J. Gosztola, D.V. Talapin, P. D. Ashby, E.V. Shevchenko, The role of order, nanocrystal size, and capping ligands in the collective mechanical response of three-dimensional nanocrystal solids, J. Am. Chem. Soc. 132 (26) (2010) 8953–8960.
[9] M. Gauvin, N.L. Yang, Z.J. Yang, I. Arfaoui, M.P. Pileni, Hierarchical mechanical behavior of cobalt supracrystals related to nanocrystallinity, Nano Res. 8 (11) (2015) 3480–3487.
[10] P. Podsiadlo, B. Lee, V.B. Prakapenka, G.V. Krylova, R.D. Schaller, A. Demortiere, E.V. Shevchenko, High-pressure structural stability and elasticity of supercrystals self-assembled from nanocrystals, Nano Lett. 11 (2) (2011) 579–588.
[11] A. Dreyer, A. Feld, A. Kornowski, E.D. Yilmaz, H. Noei, A. Meyer, T. Krekeler, C. Jiao, A. Stierle, V. Abetz, et al., Organically linked iron oxide nanoparticle supercrystals with exceptional isotropic mechanical properties, Nat. Mater. 15 (2016) 522.
[12] B. Bor, D. Giuntini, B. Domènech, M.V. Swain, G.A. Schneider, Nanoindentation-based study of the mechanical behavior of bulk supercrystalline ceramic-organic nanocomposites, J. Eur. Ceram. Soc. 39 (10) (2019) 3247–3256.
[13] X.W. Gu, Mechanical properties of architected nanomaterials made from organic–inorganic nanocrystals, JOM 70 (10) (2018) 2205–2217.
[14] M.-P. Pileni, Mechanical properties of supracrystals, EPL (Europhys. Lett.) 119 (3) (2017) 37002.
[15] S.M. Zhandarov, Edith, Christina Scheffler, Gerhard Kalinka, Claudia Poitzsch, Stefan Fliescher, Investigation of interfacial strength parameters in polymer matrix composites: compatibility and reproducibility, Adv. Ind. Eng. Polymer Res. 1 (1) (2018) 82–92.
[16] S.-L. Gao, E. Mäder, Characterisation of interphase nanoscale property variations in glass fibre reinforced polypropylene and epoxy resin composites, Compos. Appl. Sci. Manuf. 33 (4) (2002) 559–576.
[17] D. Ciprari, K. Jacob, R. Tannenbaum, Characterization of polymer nanocomposite interphase and its impact on mechanical properties, Macromolecules 39 (19) (2006) 6565–6573.
[18] J. Jancar, Review of the role of the interphase in the control of composite performance on micro- and nano-length scales, J. Mater. Sci. 43 (20) (2008) 6747–6757.
[19] N. Sheng, M.C. Boyce, D.M. Parks, G.C. Rutledge, J.I. Abes, R.E. Cohen, Multiscale micromechanical modeling of polymer/clay nanocomposites and the effective clay particle, Polymer 45 (2) (2004) 487–506.
[20] I. Sevostianov, M. Kachanov, Effect of interphase layers on the overall elastic and conductive properties of matrix composites. Applications to nanosize inclusion, Int. J. Solid Struct. 44 (3) (2007) 1304–1315.
[21] S. Ma, I. Scheider, S. Bargmann, Continuum damage modeling and simulation of hierarchical dental enamel, Model. Simulat. Mater. Sci. Eng. 24 (4) (2016), 045014.
[22] S. Ma, I. Scheider, S. Bargmann, Anisotropic constitutive model incorporating multiple damage mechanisms for multiscale simulation of dental enamel, J. Mech. Behav. Biomed. Mater. 62 (2016) 515–533.
[23] M. Li, J. Füssl, M. Lukacevic, J. Eberhardsteiner, C.M. Martin, Strength predictions of clear wood at multiple scales using numerical limit analysis approaches, Comput. Struct. 196 (2018) 200–216.
[24] V. Cannillo, F. Bondioli, L. Lusvarghi, M. Montorsi, M. Avella, M.E. Errico, M. Malinconico, Modeling of ceramic particles filled polymer–matrix nanocomposites, Compos. Sci. Technol. 66 (7) (2006) 1030–1037.
[25] R. Qiao, L.C. Brinson, Simulation of interphase percolation and gradients in polymer nanocomposites, Compos. Sci. Technol. 69 (3) (2009) 491–499.

[26] A. Pontefisso, M. Zappalorto, M. Quaresimin, An efficient RVE formulation for the analysis of the elastic properties of spherical nanoparticle reinforced polymers, Comput. Mater. Sci 96 (2015) 319–326.
[27] B. Mortazavi, J. Bardon, S. Ahzi, Interphase effect on the elastic and thermal conductivity response of polymer nanocomposite materials: 3D finite element study, Comput. Mater. Sci. 69 (2013) 100–106.
[28] R.D. Peng, H.W. Zhou, H.W. Wang, L. Mishnaevsky, Modeling of nano-reinforced polymer composites: Microstructure effect on Young's modulus, Comput. Mater. Sci. 60 (2012) 19–31.
[29] W. Wang, K. Sadeghipour, G. Baran, Finite element analysis of the effect of an interphase on toughening of a particle-reinforced polymer composite, Appl. Sci. Manufact. 39 (6) (2008) 956–964.
[30] M. Quaresimin, M. Salviato, M. Zappalorto, A multi-scale and multi-mechanism approach for the fracture toughness assessment of polymer nanocomposites, Compos. Sci. Technol. 91 (2014) 16–21.
[31] M. Zappalorto, M. Salviato, M. Quaresimin, Influence of the interphase zone on the nanoparticle debonding stress, Compos. Sci. Technol. 72 (1) (2011) 49–55.
[32] S. Ma, I. Scheider, S. Bargmann, Ultrastrong nanocomposites with interphases: nonlocal deformation and damage behavior, Eur. J. Mech. Solid. 75 (2019) 93–108.
[33] D. Santos-Carballal, A. Roldan, R. Grau-Crespo, N.H. de Leeuw, A DFT study of the structures, stabilities and redox behaviour of the major surfaces of magnetite Fe3O4, Phys. Chem. Chem. Phys. 16 (39) (2014) 21082–21097.
[34] J. Reichmann Hans, D. Jacobsen Steven, High-pressure elasticity of a natural magnetite crystal, Am. Mineral. 89 (7) (2004) 1061–1066.
[35] C. González, J. Llorca, Mechanical behavior of unidirectional fiber-reinforced polymers under transverse compression: microscopic mechanisms and modeling, Compos. Sci. Technol. 67 (13) (2007) 2795–2806.
[36] M. Herráez, D. Mora, F. Naya, C.S. Lopes, C. González, J. Llorca, Transverse cracking of cross-ply laminates: a computational micromechanics perspective, Compos. Sci. Technol. 110 (2015) 196–204.
[37] L. Yang, Y. Yan, Y. Liu, Z. Ran, Microscopic failure mechanisms of fiber-reinforced polymer composites under transverse tension and compression, Compos. Sci. Technol. 72 (15) (2012) 1818–1825.
[38] P. Stempfle, O. Pantale, M. Rousseau, E. Lopez, X. Bourrat, Mechanical properties of the elemental nanocomponents of nacre structure, Mater. Sci. Eng. C-Mater. Biol. Appl. 30 (5) (2010) 715–721.
[39] B. Domenech, A. Plunkett, M. Kampferbeck, M. Blankenburg, B. Bor, D. Giuntini, T. Krekeler, M. Wagstaffe, H. Noei, A. Stierle, et al., Modulating the mechanical properties of supercrystalline nanocomposite materials via solvent-ligand interactions, Langmuir 35 (43) (2019) 13893–13903.
[40] L. Djumas, A. Molotnikov, G.P. Simon, Y. Estrin, Enhanced mechanical performance of bio-inspired hybrid structures utilising topological interlocking geometry, Sci. Rep. 6 (2016) 26706.
[41] T. Hugel, M. Rief, M. Seitz, H.E. Gaub, R.R. Netz, Highly stretched single polymers: atomic-force-microscope experiments versus ab-initio theory, Phys. Rev. Lett. 94 (4) (2005), 048301.
[42] D. Giuntini, E. Torresani, K.T. Chan, M. Blankenburg, L. Saviot, B. Bor, B. Domènech, M. Shachar, M. Müller, E.A. Olevsky, et al., Iron oxide-based nanostructured ceramics with tailored magnetic and mechanical properties: development of mechanically robust, bulk superparamagnetic materials, Nanoscale Adv. 1 (2019) 3139–3150.